

Ratchet current in a \mathcal{PT} -symmetric Floquet quantum system with symmetric sinusoidal drivingZhiqiang Li,¹ Xiaoxiao Hu¹, Jinpeng Xiao,² Yajiang Chen¹, and Xiaobing Luo^{1,2,*}¹*Department of Physics, Zhejiang Sci-Tech University, Hangzhou 310018, China*²*School of Mathematics and Physics, Jinggangshan University, Ji'an 343009, China*

(Received 27 June 2023; accepted 23 October 2023; published 9 November 2023)

We consider the ratchet dynamics in a \mathcal{PT} -symmetric Floquet quantum system with symmetric temporal (harmonic) driving. In the exact \mathcal{PT} -symmetry phase, for a finite number of resonant frequencies, we show that the long-lasting resonant currents can be generated with the symmetric time-continuous driving, which would otherwise forbid the generation of directed currents in the Hermitian limit. Such a non-Hermitian resonant current can be enhanced by increasing the non-Hermitian level and, in particular, the resonant current peaks (reaches the largest negative value) under the condition that the imaginary part of the potential depth is equal to the real part, at which the stable asymptotic current occurs owing to exceptional points mechanism. Moreover, the directed currents originating from the symmetry breaking are reported, which increase linearly with the driving frequency, the mechanism behind which is that the cutoff of the momentum eigenstates for the Floquet state with maximum imaginary quasienergy increases as the driving frequency is continuously increased. We also present a non-Hermitian three-level model that can account for the resonant currents and gives surprisingly good agreement with direct numerical results for weak driving, even in the broken- \mathcal{PT} -symmetry regime for the first-order resonance. Our results provide a means of realizing the non-Hermiticity-controlled ratchet current by means of a smooth continuous driving, previously used only to generate currents in Hermitian systems.

DOI: [10.1103/PhysRevA.108.052211](https://doi.org/10.1103/PhysRevA.108.052211)**I. INTRODUCTION**

The ratchet effect, that is, directed transport under a zero mean force, has attracted a continuous interest over the past few decades. This is due to its fundamental and practical importance: on the one hand, its mechanism is relevant to the understanding of quantum chaos and quantum-classical correspondence [1–5], and on the other hand, it has found diverse applications in many fields, from mechanical devices to quantum systems [6–10]. To achieve the ratchet effects, the system must be driven out of equilibrium, and relevant spatiotemporal symmetries, which would otherwise prevent the formation of a directed current, must be broken [2,4,11,12]. Aside from the classical ratchets, the ratchet phenomenon has also been extended to the quantum regime as it is of great importance, for example, in the design of coherent nanoscale devices [7,13]. Due to the high degree of quantum control, Bose-Einstein condensates (BECs) of dilute gases loaded into optical lattices have proven to be excellent candidates for the study of such coherent ratchet effects. Considerable progress has been made in this direction through the study of the quantum kicked rotor [14–19], a paradigm of quantum chaos, which can be realized by exposing a sample of cold atoms to short pulses of an optical standing wave [20]. Other schemes and proposals to implement directed (ratchet) quantum transport in BECs involve the use of time-continuous driving [2–5,21], which has the advantage of being less heating than kick-type driving [21]. Directed transport in the presence of nonlinearity arising from

the many-body nature of BECs has also been investigated in the literature [22–27], where it has been found that the interactions between atoms can be harnessed to generate directed transport even when time-reversal symmetry holds [24].

So far, most investigations of the quantum ratchet effect have been performed in the context of Hermitian dynamics. The Hermiticity requirement of a Hamiltonian guarantees its real energy eigenvalues and the conserved total probability. However, a large class of non-Hermitian Hamiltonians that are parity-time symmetric (\mathcal{PT} symmetric) can still have completely real eigenvalue spectra as long as they commute with the parity-time operator [28–34]. One of the most interesting results of such \mathcal{PT} -symmetric non-Hermitian Hamiltonian systems is the phase (symmetry-breaking) transition, where the spectrum changes from all real (the exact \mathcal{PT} phase) to complex (the broken- \mathcal{PT} -symmetry phase) when the non-Hermitian parameter exceeds a certain threshold [28–31]. At the transition, the system has exceptional points, also called non-Hermitian degeneracies, at which both the eigenvalues and the eigenvectors of the underlying system coalesce, giving rise to many counterintuitive phenomena [35–45]. The study of \mathcal{PT} -symmetric systems has recently been extended to systems with periodically driven potentials (Floquet systems), where the quasienergy (Floquet) spectrum takes the place of the energy spectrum of the static systems [46–68]. A prototype example is the \mathcal{PT} -symmetric kicked rotor (KR), where chaos has been shown to assist the exact \mathcal{PT} phase [46]. The transport properties in such \mathcal{PT} -symmetric KR have also attracted some attention in recent years [69–71]. For example, a type of non-Hermitian unidirectional transport, called non-Hermitian accelerator modes, has been discovered

*xiaobingluo2013@aliyun.com

in the delocalized regime (quantum resonances) for a \mathcal{PT} -symmetry extension of the KR model [69]. Additionally, directed momentum current induced by the \mathcal{PT} -symmetric driving in the KR model has been investigated [70]. More recently, Ref. [72] has proposed a scheme for generating a persistent current using a static non-Hermitian ratchet. However, knowledge of the quantum ratchet effect in \mathcal{PT} -symmetric Floquet systems with time-continuous driving (i.e., a potential that varies smoothly with time rather than being pulsed) is still largely unknown, which from a theoretical point of view may be due to the greater analytical challenges and difficulties involved than with pulsed-type driving. In reality, time-continuous driving excites fewer high-momentum modes and generates less heating than kick-type driving, thus better preserving atomic coherence and quantum effects in the experiment, which is also one of the reasons for using time-continuous driving in this work.

In this paper, we investigate the ratchet currents in a \mathcal{PT} -symmetric Floquet system with symmetric time-continuous driving. In the exact \mathcal{PT} -symmetry phase, although the system is conservative on average, we find that the persistent ratchet current can be generated for a finite set of resonant driving frequencies. Such a resonant ratchet current is a hallmark of non-Hermitian transport, as it would disappear in the Hermitian limit. This means that to generate such a non-Hermitian resonant current, no sawtoothlike asymmetric temporal driving is required. We show that the resonant current can be enhanced by increasing the non-Hermitian level. This is because the time evolution of the current exhibits a square-wave-like shape as the non-Hermitian level increases, which is drastically different from the Rabi-type oscillation in the Floquet-Hermitian system [2,21]. The time-averaged current peaks (reaches a maximum) when the imaginary part of the potential depth is equal to the real part, at which the stable asymptotic current exists due to exceptional points (EPs) mechanism. It is found that the maximum value of the non-Hermitian resonant current exists at the EPs for a series of discrete frequencies, i.e., the value of the driving frequencies equal to a half-integer or an integer, which can either correspond to the \mathcal{PT} -symmetry-breaking points or, surprisingly, arise as an isolated parameter point deep in the unbroken- \mathcal{PT} -symmetry regime. A non-Hermitian three-level model can be used to capture the resonant current, and gives a surprisingly good agreement with the numerically exact results for the weak driving. In the broken- \mathcal{PT} -symmetry regime, it is shown that the asymptotic current increases linearly with the driving frequency. The underlying physics is that, after sufficient evolution time, the system is dominated by the Floquet states whose quasienergy has the largest imaginary part, and the cut-off of the momentum mode of this Floquet state also increases with increasing driving frequency. Finally, the nonlinearity effects on the directed current at EPs are also discussed.

The paper is organized as follows. In Sec. II, we describe the model system and show that the introduction of non-Hermiticity gives rise to the Floquet states with asymmetric momentum distribution. In Sec. III, we study the non-Hermitian resonant currents both numerically and analytically. In Sec. IV, the directed currents due to EPs mechanism are identified. In Sec. V, the directed currents originating from the symmetry breaking are reported, which are found

to increase linearly with the driving frequency. In Sec. VI, we show that the non-Hermitian directed current can be induced or suppressed by introducing nonlinearity. The results are summarized in Sec. VII.

II. MODEL AND CURRENT-CARRYING FLOQUET EIGENSTATES

We consider condensed atoms confined in a toroidal trap, where the thickness r of the toroidal trap is much smaller than its radius R , so that lateral motion is neglected and the system is essentially one dimensional. Hence, our problem is described by the dimensionless nonlinear Gross-Pitaevskii (GP) equation (taking $\hbar = m = 1$)

$$i \frac{\partial}{\partial t} \psi(x, t) = \left[\frac{\hat{p}^2}{2} + g |\psi(x, t)|^2 + V(x, t) \right] \psi(x, t), \quad (1)$$

where x is the coordinate, $\hat{p} = -i\partial/\partial x$ is the angular-momentum operator, $g = 8NaR/r$ is the scaled strength of nonlinear interaction, N is the number of atoms, and a is the s -wave scattering length for elastic atom-atom collisions. The condensate is driven by a complex external potential which is periodic in time and has a zero mean, reading as

$$V(x, t) = K[\sin x + i\lambda \cos(x + \phi)] \sin(\omega t), \quad (2)$$

where K and ω denote the strength and angular frequency of the flashing potential, ϕ is the initial spatial phase of the non-Hermitian potential (in our investigation, we will set $\phi = 0$, and introducing the initial phase can be used to change the plus-minus sign of the mean currents, thereby steering the transport direction), and $\lambda > 0$ is the non-Hermitian parameter measuring the strength of the imaginary part of the potential. Throughout this paper, we measure all energies in units of $\hbar^2/2mR^2$, and our analysis will focus mostly on the linear case ($g = 0$) unless explicitly stated otherwise. One can easily verify that the considered Hamiltonian is \mathcal{PT} symmetric since the system is invariant under the combined action of the parity operator $\hat{P} : x \rightarrow -x$ and the time-inversion operator $\hat{T} : i \rightarrow -i, t \rightarrow -t$.

In Eq. (1), the periodic boundary condition $\psi(x, t) = \psi(x + 2\pi, t)$ allows us to expand the wave function as $|\psi(t)\rangle = \sum_{n=-\infty}^{\infty} c_n(t) |n\rangle$, where $|n\rangle = \frac{1}{\sqrt{2\pi}} e^{inx}$ denotes an eigenstate of the undriven Hamiltonian with (quantized) momentum $n\hbar$.

The time evolution of a quantum state over one period $T = 2\pi/\omega$ is governed by the Floquet operator

$$\hat{U}(t + T, t) = \hat{T} e^{-i \int_t^{t+T} dt \hat{H}(t)}, \quad (3)$$

where \hat{T} stands for the time-ordering operator. The eigenequation of the Floquet operator reads as

$$\hat{U}(t + T, t) |\phi_\alpha(t)\rangle = e^{-i\varepsilon_\alpha T} |\phi_\alpha(t)\rangle, \quad (4)$$

where ε_α indicates the quasienergy and $|\phi_\alpha(t)\rangle$ the Floquet mode. As in the undriven case, the Floquet \mathcal{PT} -symmetric system is said to be in the unbroken- \mathcal{PT} -symmetry phase if the quasienergies are entirely real, while it is said to be in the broken- \mathcal{PT} -symmetry phase if complex-conjugate quasienergies emerge when λ exceeds a certain threshold, i.e.,

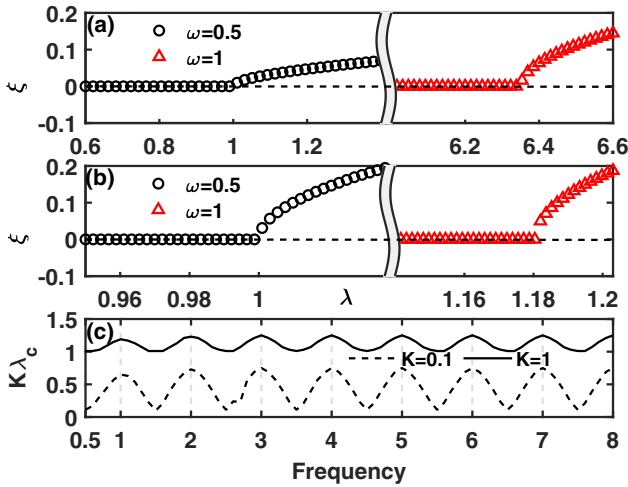


FIG. 1. The sum of the absolute values of the imaginary parts of the quasienergies $\xi = \sum_{\alpha=1}^N |\varepsilon_{\alpha}^i|$ versus the non-Hermitian parameter λ for (a) weak driving $K = 0.1$; (b) strong driving $K = 1$. Here ξ is shown for two driving frequencies $\omega = 0.5$ (black circles) and $\omega = 1$ (red triangles) for each K . For $\omega = 0.5$, \mathcal{PT} -symmetry breaking is clearly observed at $\lambda_c = 1$ for both weak and strong driving. However, for $\omega = 1$, the \mathcal{PT} -symmetry-breaking points are different for weak ($\lambda_c = 6.34$) and strong ($\lambda_c = 1.181$) driving. (c) Threshold $K\lambda_c$ versus driving frequency ω for a weak driving ($K = 0.1$) and a strong driving ($K = 1$). In the numerical calculation, ξ is summed up over the $N = 512$ Floquet modes. Quantities plotted in all the figures are dimensionless.

$\lambda > \lambda_c$. Such a phase transition is referred to as \mathcal{PT} -symmetry breaking.

To identify such a spontaneous \mathcal{PT} -symmetry breaking, we numerically compute the sum of the absolute values of the imaginary parts of all quasienergies (see Fig. 1),

$$\xi = \sum_{\alpha=1}^N |\varepsilon_{\alpha}^i|, \quad (5)$$

where the Floquet matrix is truncated with $N = 512$ in momentum space, and ε_{α}^i denotes the imaginary part of the α th quasienergy. More accurate numerical diagonalization calculations are presented in the Refs. [73,74]. Figure 1 shows the numerical behavior of the sum of $|\varepsilon_{\alpha}^i|$ as a function of the non-Hermitian parameter λ for weak driving $K = 0.1$ [Fig. 1(a)] and strong driving $K = 1$ [Fig. 1(b)]. There is indeed a threshold λ_c above which the sum of $|\varepsilon_{\alpha}^i|$ increases from zero to a nonzero value, representing a spontaneous \mathcal{PT} -symmetry breaking, as shown in Figs. 1(a) and 1(b). Additionally, the \mathcal{PT} -symmetry-breaking threshold varies with the driving frequency. The dependence of the \mathcal{PT} -symmetry-breaking threshold on the driving frequency is also plotted in Fig. 1(c), where we observe that the \mathcal{PT} -symmetry-breaking threshold varies almost periodically with the driving frequency, i.e., it reaches a maximum when ω takes integer values and instead reaches a minimum when ω takes half-integer values. We also observe that the threshold $K\lambda$ for \mathcal{PT} -symmetry breaking increases with the driving strength K .

Let us have a look at the properties of the Floquet state that shed light on the understanding of the transport

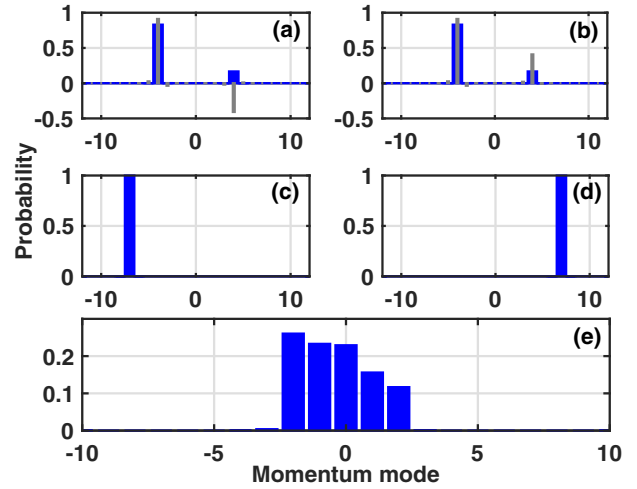


FIG. 2. Occupation of the momentum modes for three types of Floquet states in the unbroken- \mathcal{PT} -symmetry regime. The blue bars are for the population probabilities in different momentum modes, and the gray thin bars [see (a) and (b)] are for the distribution of the real parts of the amplitudes in different momentum modes for corresponding Floquet states. (a), (b) Correspond to a pair of degenerate Floquet states with the same momentum occupation, but with different real parts of the probability amplitudes. (c), (d) A pair of degenerate Floquet states that occupy the momentum modes in a symmetric manner. These two types have no contribution to the current because of no projection onto the initial state $|0\rangle$. (e) A typical example of a nondegenerate Floquet state that carries a current and overlaps with the initial state. The parameters are $K = 1$, $\omega = 1$, and $\lambda = 0.1$.

phenomenon. To better distinguish between non-Hermitian and Hermitian situations, we first concentrate on the Floquet states in the unbroken- \mathcal{PT} -symmetry phase, where the quasienergy spectrum is entirely real. In this case, our numerical results show that the Floquet states fall into two classes, degeneracy and nondegeneracy. The momentum distributions of these two typical Floquet states are shown in Fig. 2. These degenerate Floquet states appear as doublets, which are of two kinds: the pair of degenerate Floquet states that occupy the same momentum component but with different real parts (marked by gray thin bars), as shown in Figs. 2(a) and 2(b), and the pair of degenerate Floquet states that occupy the negative and positive momentum components in a symmetric manner, as shown in Figs. 2(c) and 2(d). In this paper, we assume that the system is initially prepared in the zero-current state $|0\rangle$, which is experimentally convenient because it is the ground state of the undriven Hamiltonian. With such an initial preparation, none of these degenerate states will contribute to the current since they are well localized in the momentum space and have no projection onto the initial state. Furthermore, our numerical results reveal that all nondegenerate Floquet states have asymmetric momentum distributions around the mode $|0\rangle$, thus acquiring nonzero mean momentum and becoming transporting. A representative example of such a nondegenerate Floquet state is illustrated in Fig. 2(e). Due to their asymmetric nature, it is reasonable to expect that these nondegenerate Floquet states would give origin to the directed currents of the Floquet \mathcal{PT} -symmetry system in the

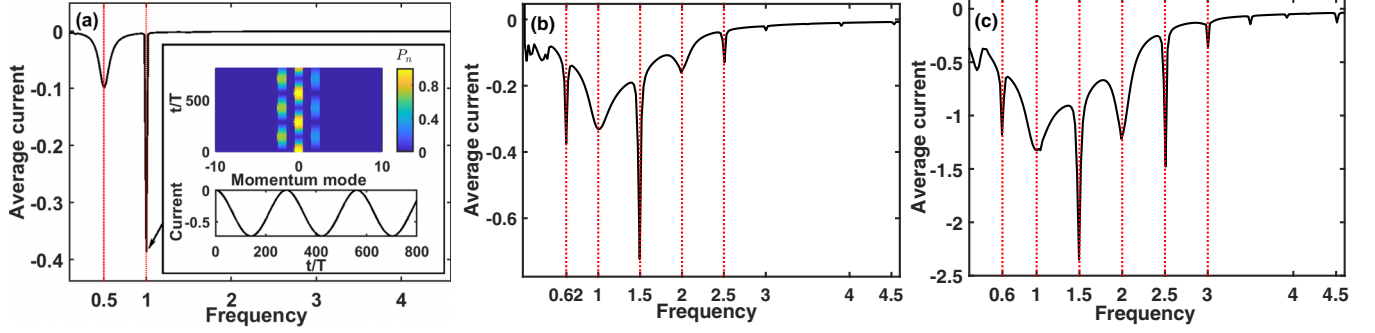


FIG. 3. Time-averaged current (TAC), plotted as a function of the driving frequency ω . (a) TAC for weak driving with $K = 0.1$ and $\lambda = 0.1$. The TAC peaks only at $\omega = 0.5$ and 1 , in agreement with the resonance condition $\frac{n^2}{2} = m\omega$, representing the first- and the second-order dynamics, respectively. (b) TAC for strong driving with $K = 1$ and $\lambda = 0.1$. More resonances are observed for the strong driving and the pronounced resonance is shifted from $\omega = 1$ to 1.5 . (c) The same as in (b), but with a strong non-Hermitian parameter $\lambda = 0.5$. As we can see, the TAC at resonant frequencies is significantly enhanced by increasing the non-Hermitian strength λ . Insets in (a) are for the detailed current behavior at $\omega = 1$ resonance: top: time evolution of the populations P_n in momentum space; bottom: Rabi oscillation of the current $I(t)$.

unbroken- \mathcal{PT} -symmetry phase. Finally, we should point out that in the Hermitian limit $\lambda \rightarrow 0$, where directed current generation is forbidden, these asymmetric Floquet states can no longer exist.

At the \mathcal{PT} -symmetry phase transition point, also known as so-called exceptional point (EP), not only the quasienergies but also the Floquet states become the same. Thus, due to the singularity at the EP, we cannot expand the quantum state on the basis of the Floquet states, nor can we study the time evolution of the current only by means of the analysis of the Floquet states. However, some analytical solutions for currents at EPs can be given in this paper (see Sec. IV for details). In the broken- \mathcal{PT} -symmetry phase, the dynamics of the ratchet current is dominated by the Floquet states, the quasienergy of which has the largest imaginary part; more details will be given in Sec. V.

III. NON-HERMITIAN RESONANT CURRENTS

To start out, we introduce the asymptotic time-averaged current (TAC), which is defined as

$$\bar{I} = \lim_{t \rightarrow \infty} \frac{1}{t} \int_{t_0=0}^t dt' I(t'), \quad (6)$$

where the current $I(t)$ is given by

$$I(t) = \frac{\int_0^{2\pi} dx \psi^*(x, t) \hat{p} \psi(x, t)}{\mathcal{N}(t)}, \quad (7)$$

with $\mathcal{N}(t) = \int_0^{2\pi} dx |\psi(x, t)|^2$ being the norm of the quantum state [69].

In this section, we are particularly interested in a special type of transport phenomenon in the Floquet \mathcal{PT} -symmetric system when the conditions for quantum resonance are fulfilled, i.e., $\frac{n^2}{2} = m\omega$, where $\frac{n^2}{2}$ is the unperturbed level difference between $|0\rangle$ and $|n\rangle$. The resonance condition is referred to as the integer multiples of the driving frequency equal to the energy-level gap between the unperturbed initial states and the resonant states. Physically, if the energy of m photons $m\omega$ matches the gap, the system is capable of absorbing photons of sufficient energy to bridge the

energy difference $n^2/2$ between the unperturbed levels, through which the quantum transition takes place. Mathematically, with the resonance condition, the dynamics is mainly limited in the degenerate subspace of the extended Hilbert space under the weak driving.

In Fig. 3, we numerically study the TAC over a wide range of driving frequencies with fixed driving strength, focusing on the case of unbroken- \mathcal{PT} -symmetry phase. Figure 3(a) shows clear signatures of resonant currents at $\omega = 0.5, 1$, for weak driving $K = 0.1$, where the pronounced resonance at $\omega = 1$ arises from the mixing between $|0\rangle$ (the initial state) and the current-carrying mode $|\pm 2\rangle$ (see the insets). For strong driving $K = 1$, we find that more resonant currents are visible and the position of the pronounced resonance is shifted to $\omega = 1.5$, as shown in Fig. 3(b). This is obvious because strong driving will excite a larger number of higher momentum modes. Meanwhile, if we keep $K = 1$ unchanged and increase the non-Hermitian strength λ , we observe that the resonant currents are preserved and that the position of the pronounced resonance does not shift with increasing non-Hermitian strength, as can be seen in Fig. 3(c). More interestingly, it can be seen from the comparison of Figs. 3(b) and 3(c) that non-Hermiticity enhances the resonant currents.

The generation of resonant currents in the \mathcal{PT} -symmetric system is essentially due to the time-reversal symmetry breaking induced by the introduction of non-Hermiticity. This is in contrast to the scheme for achieving directed current in Hermitian systems, where a ratchet potential with asymmetric temporal driving is required to simultaneously break the time-reversal and space-inversion symmetries [2,21]. In what follows, we attempt to understand such non-Hermitian resonant currents by means of the well-established Floquet theory. In the basis of the Floquet eigenstates, an arbitrary time-evolved quantum state can be expanded as

$$|\psi(t)\rangle = \sum_{\alpha} C_{\alpha} e^{-i\varepsilon_{\alpha} t} |\phi_{\alpha}(t)\rangle, \quad (8)$$

where C_{α} is the projection coefficient of the initial state onto the Floquet state $|\phi_{\alpha}(0)\rangle$, such that $C_{\alpha} = \langle \phi_{\alpha}(0) | \psi(0) \rangle$. Thus, in the unbroken- \mathcal{PT} -symmetry phase, the momentum

expectation value is given by

$$\begin{aligned} \langle p(t) \rangle &= \sum_{\alpha' \neq \alpha} C_{\alpha'}^* C_{\alpha} e^{i(\varepsilon_{\alpha'} - \varepsilon_{\alpha})t} \langle \phi_{\alpha'}(t) | \hat{p} | \phi_{\alpha}(t) \rangle \\ &= \sum_{\alpha} |C_{\alpha}|^2 \langle \phi_{\alpha}(t) | \hat{p} | \phi_{\alpha}(t) \rangle \\ &\quad + \sum_{\alpha' \neq \alpha} C_{\alpha'}^* C_{\alpha} e^{i(\varepsilon_{\alpha'} - \varepsilon_{\alpha})t} \langle \phi_{\alpha'}(t) | \hat{p} | \phi_{\alpha}(t) \rangle, \end{aligned} \quad (9)$$

where $\langle \phi_{\alpha}(t) | \hat{p} | \phi_{\alpha}(t) \rangle$ is the mean instantaneous momentum of the Floquet state, which is a periodic function due to $|\phi_{\alpha}(t)\rangle = |\phi_{\alpha}(t+T)\rangle$. In cases other than exact degeneracies, the off-diagonal interference terms $\exp[i(\varepsilon_{\alpha'} - \varepsilon_{\alpha})t]$ would average to zero for long enough times, and the contributions to the directed current are given only by the diagonal terms $\langle \sum_{\alpha} |C_{\alpha}|^2 \langle \phi_{\alpha} | \hat{p} | \phi_{\alpha} \rangle_T$, where $\langle \dots \rangle_T$ denotes the time average over the period T . Since the non-Hermitian driving potential breaks time-reversal symmetry, there exist asymmetric Floquet states in the unbroken- \mathcal{PT} -symmetry phase, which can be either degenerate or nondegenerate, as we have shown in Fig. 2. Despite the existence of the degenerate Floquet states, which are well localized in momentum space, they do not overlap with the initial state $|0\rangle$, i.e., the corresponding expansion coefficients C_{α} are zero, thus having no consequence on the currents. In our model, the numerical results show that all the asymmetric nondegenerate Floquet states overlap with the initial state $|0\rangle$ and have a negative mean momentum, which contributes to the diagonal terms ($\alpha = \alpha'$) in Eq. (9), thus leading to the appearance of directed currents as shown in Fig. 3.

As shown in Fig. 3, the non-Hermitian ratchet current can be significantly increased for a finite set of resonant driving frequencies. To give an excellent account of the resonant currents, we follow the perturbative method of [21] and generalize it to the non-Hermitian model, which is found to be in surprisingly good agreement with numerical results. Our starting point for the study is given by the unperturbed Floquet states $|n, m\rangle = \frac{1}{\sqrt{2\pi T}} e^{inx} e^{-im\omega t}$, which are Floquet eigenstates of the unperturbed Floquet Hamiltonian $\frac{\hat{p}^2}{2} - i\partial/\partial t$, with the Floquet quasienergies $\varepsilon = \frac{n^2}{2} - m\omega$. When the initial state is prepared as the ground state of the unperturbed Hamiltonian, which corresponds to the Floquet state $|0, 0\rangle$, we may expect the driving to mix $|0, 0\rangle$ with the other unperturbed Floquet states $|n, m\rangle$ satisfying the resonance condition $m = \frac{n^2}{2\omega}$. For example, for the case $\omega = 1$, the system is expected to evolve from $|0, 0\rangle$ towards $|2, 2\rangle$ and $|\bar{2}, 2\rangle$ (for notational brevity, we use $\bar{n} \equiv -n$), where the mixing with the higher-lying ($n > 2$) resonant Floquet states is very small and can be neglected under weak driving. Thus, when $\omega = 1$, truncating the Hilbert space to just these three resonant states $\{|2, 2\rangle, |0, 0\rangle, |\bar{2}, 2\rangle\}$ is sufficient to describe the dynamics under weak driving.

By applying the time-independent perturbation theory in the extended Hilbert space spanned by the relevant three resonant Floquet states $\{|2, 2\rangle, |0, 0\rangle, |\bar{2}, 2\rangle\}$, the dynamics of the system can be described by an effective three-level non-Hermitian model for $\omega = 1$ (more details can be seen in the

Appendix):

$$T \simeq \begin{bmatrix} 0 & \Gamma_- & 0 \\ \Gamma_+ & 0 & \Gamma_- \\ 0 & \Gamma_+ & 0 \end{bmatrix}, \quad (10)$$

where $\Gamma_{\pm} = K^2 \lambda_{\pm}^2 / 8$ and $\lambda_{\pm} \equiv \lambda \pm 1$. We can see that the effective T matrix is non-Hermitian due to $\lambda \neq 0$. By solving the Schrödinger equation on the basis of the effective three-level model, we obtain the time evolution of the populations on the momentum eigenstates as follows:

$$\begin{aligned} P_2(t) &= \frac{\Gamma_-^2}{\Omega^2} \sin^2(\Omega t), \\ P_0(t) &= \cos^2(\Omega t), \\ P_{-2}(t) &= \frac{\Gamma_+^2}{\Omega^2} \sin^2(\Omega t), \end{aligned} \quad (11)$$

where P_n denotes the population in the momentum mode $|n\rangle$, and the Rabi oscillation frequency is given by $\Omega = \sqrt{2\Gamma_- \Gamma_+}$. The corresponding norm thus reads as $\mathcal{N}(t) = P_{-2} + P_0 + P_2 = \cos^2 \Omega t + \frac{\Gamma_-^2 + \Gamma_+^2}{\Omega^2} \sin^2 \Omega t$. By definition, Eq. (7), after omitting the contribution of the norm to the current behavior, the current is given by

$$I(t) = \frac{-2(\Gamma_+^2 - \Gamma_-^2)}{(\Gamma_+^2 + \Gamma_-^2) + \Omega^2 \cot^2(\Omega t)}. \quad (12)$$

When the non-Hermitian strength $\lambda = 0$ is zero, we have $\Gamma_+ = \Gamma_-$ such that $I(t) = 0$, which is a natural consequence due to the fact that the limit of $\lambda \rightarrow 0$ leads to the recovery of the time-reversal symmetry. In this way, we analytically confirm the conclusion that the non-Hermiticity produces the resonant current in the system with symmetric temporal driving, which would otherwise forbid the generation of direct currents. Note that as soon as the non-Hermitian term is switched, the ratchet current appears, regardless of whether the system has \mathcal{PT} symmetry or not. However, for the specific \mathcal{PT} -symmetric driving potential, as will be shown later, there is a rich variety of current dynamics in different phase regions (invariant \mathcal{PT} symmetry, EPs, and broken \mathcal{PT} symmetry).

Considering the other resonant frequency $\omega = 0.5$, the weakly driven system can also be truncated to an effective three-level model operating in a reduced Hilbert space of resonant Floquet states $|n, m\rangle = \{|1, 1\rangle, |0, 0\rangle, |\bar{1}, 1\rangle\}$. The corresponding effective T matrix is given by

$$T \simeq \begin{bmatrix} 0 & -\Gamma'_- & 0 \\ -\Gamma'_+ & 0 & \Gamma'_- \\ 0 & \Gamma'_+ & 0 \end{bmatrix}, \quad (13)$$

where $\Gamma'_{\pm} = K(1 \pm \lambda)/4$. A comparison of the T matrices at $\omega = 0.5$ and 1 shows that the effective coupling Γ_{\pm} is proportional to K^2 when $\omega = 1$, while when $\omega = 0.5$, the effective coupling Γ'_{\pm} is proportional to K . This is because for $\omega = 1$ the mixing between $|0, 0\rangle$ and the states $|2, 2\rangle$ and $|\bar{2}, 2\rangle$ is the second-order transition via the virtual intermediate states $|1, 1\rangle$ and $|\bar{1}, 1\rangle$, whereas for $\omega = 0.5$ the mixing between $|0, 0\rangle$ and the states $|1, 1\rangle$ and $|\bar{1}, 1\rangle$ is the direct, first-order transition. Following the same line of reasoning as

above, we can obtain the populations in the momentum modes $|0\rangle$ and $|\pm 1\rangle$, from which we can further obtain the norm $\mathcal{N}(t) = \frac{\Gamma_+^2 + \Gamma_-^2}{|\Omega|^2} |\sin(\Omega t)|^2 + |\cos(\Omega t)|^2$, and the current as

$$I'(t) = -\frac{\Gamma_+^2 - \Gamma_-^2}{(\Gamma_+^2 + \Gamma_-^2) + |\Omega|^2 |\cot(\Omega t)|^2}, \quad (14)$$

in which $\Omega' = \sqrt{2\Gamma'_- \Gamma'_+}$.

Let us further examine the second-order dynamics for the $\omega = 1$ resonance and the first-order dynamics for the $\omega = 0.5$ resonance. For the former, the Rabi oscillation frequency $\Omega = \sqrt{2\Gamma_- \Gamma_+}$, which corresponds to the quasienergy of the original time-periodic system (1) treated accurately up to the second order, is always real, whereas for the latter, $\Omega' = \sqrt{2\Gamma'_- \Gamma'_+}$, which is the first-order quasienergy of the original system (1), becomes purely imaginary when $\lambda > 1$. As such, the analytical current (12) for $\omega = 1$ resonance marks a periodic oscillation, implying that the second-order process can only describe the unbroken- \mathcal{PT} -symmetry phase dynamics. On the other hand, for the $\omega = 0.5$ resonance, as λ is increased beyond the parameter point $\lambda = 1$, the periodic oscillation of the current [see Eq. (14)] disappears and is replaced by a hyperbolic behavior, with the norm growing exponentially and the current approaching an asymptotic value of -1 . This implies that $\lambda = 1$ signals the onset of a \mathcal{PT} -symmetry phase transition for the $\omega = 0.5$ resonance, which agrees exactly with the numerical results shown in Sec. II for weak driving, and at the same time indicates that the perturbative analytical formula for the first-order process is also applicable in the broken- \mathcal{PT} -symmetry phase. Currently, the analytical quasienergies (based on the effective T matrix) for the $\omega = 1$ resonance are always real and thus do not predict the \mathcal{PT} -symmetry transition point, which should be pushed to a higher-order correction to obtain more accurate quasienergies, but the process is lengthy and beyond the scope of our paper.

Figure 4 shows an extremely good agreement between the numerical results and the analytical results of the time-dependent currents and the normalized probabilities for a weak driving $K = 0.1$. Since the effective coupling $\Gamma_{\pm} \sim K^2$ for the $\omega = 1$ resonance is smaller than the one ($\Gamma'_{\pm} \sim K$) for the $\omega = 0.5$ resonance, the former oscillation period is an order of magnitude larger than the latter, and for better comparison we use different axis scales (red for $\omega = 0.5$ and black for $\omega = 1$) to show the current behaviors. As shown in Fig. 4(a), the current for the $\omega = 0.5$ resonance shows the Rabi-type oscillation, but for the $\omega = 1$ resonance, the currents show the deviation from the Rabi-type oscillation. When λ increases, the departure from Rabi-type oscillation becomes drastic, deforming into a square-wave-like shape with a significant duration of staying at a steady value of -2 for the current with $\omega = 1$ resonance. This process is accompanied by the significant duration of the normalized probability staying at $\bar{P}_{-2}(t) \approx 1$, $\bar{P}_2(t) \approx \bar{P}_0(t) \approx 0$, as shown in Fig. 4(b), implying that TAC will be enhanced upon increasing the non-Hermitian strength. In addition, in Fig. 5, we numerically investigate the TAC as a function of the non-Hermitian strength λ for both the $\omega = 0.5$ resonance [Fig. 5(a)] and the $\omega = 1$ resonance [Fig. 5(b)], which show good agreement with the analytical results derived from the effective three-level model. In both cases,

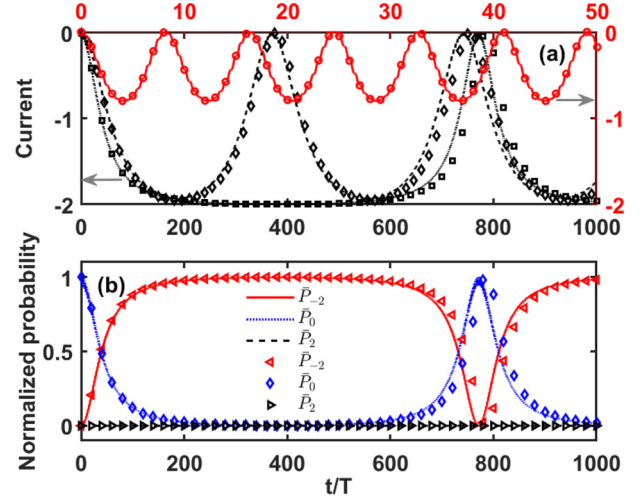


FIG. 4. Comparison of the exact numerical results (shown by lines) with the analytical results predicted by the effective three-level non-Hermitian model (circles, triangles, diamonds, and squares) in the unbroken- \mathcal{PT} -symmetry regime with weak driving $K = 0.1$. (a) Time evolution of the current $I(t)$, with different parameters $\omega = 0.5$, $\lambda = 0.5$ (solid line and circles), $\omega = 1$, $\lambda = 0.5$ (dashed line and diamonds), and $\omega = 1$, $\lambda = 0.8$ (dotted line and squares). (b) Time-dependent normalized probabilities $\bar{P}_n(t) = P_n(t)/\mathcal{N}(t)$, corresponding to the current shown by the dotted line and squares with fixed parameters $\omega = 1$, $\lambda = 0.8$.

when $\lambda < 1$, the time-averaged currents are enhanced with increasing non-Hermitian strength λ , while above the parameter point $\lambda = 1$ (marked by the green vertical line), the time-averaged currents are instead reduced with increasing non-Hermitian strength λ . The boundary $\lambda = 1$, separating

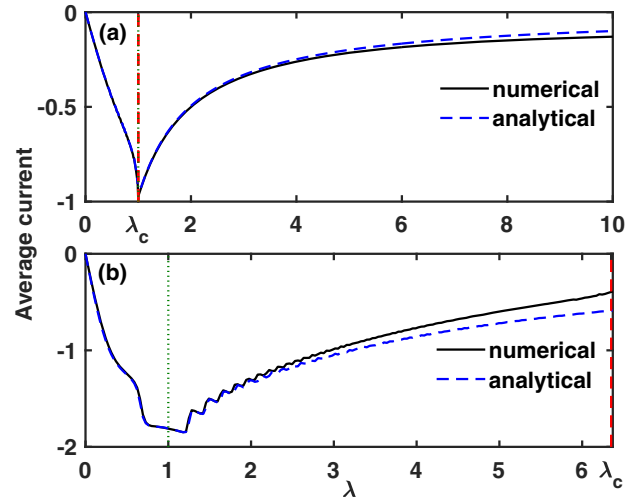


FIG. 5. Time-averaged current versus non-Hermitian parameter λ with weak driving $K = 0.1$, for (a) the $\omega = 0.5$ resonance; (b) the $\omega = 1$ resonance. The green dotted vertical lines mark the $\lambda = 1$, and the red dashed vertical lines mark the spontaneous \mathcal{PT} -symmetry-breaking threshold λ_c . We can see that for weak driving strength the agreement between the analytical results predicted by the three-level model and the exact numerical results is excellent, even in the broken- \mathcal{PT} -symmetry regime ($\lambda > 1$) for the $\omega = 0.5$ resonance.

the two regions with physically different dependence of the current on non-Hermitian strength, corresponds exactly to the symmetry-breaking point for the $\omega = 0.5$ resonance, but is located deeply in the unbroken- \mathcal{PT} -symmetry regime for the $\omega = 1$ resonance (the symmetry-breaking threshold is marked by λ_c). What is more, for the $\omega = 0.5$ resonance, the analytical result of the three-level model is still applicable in the broken- \mathcal{PT} -symmetry regime ($\lambda > 1$), showing a good agreement with the direct numerical result based on Eq. (1).

IV. DIRECTED CURRENTS AT EXCEPTIONAL POINTS

An interesting property of non-Hermitian systems is the existence of spectral singularities, known as exceptional points (EPs) [34,45], which has led to a variety of novel phenomena and fascinating applications. At this point, not only are the eigenvalues identical, but also the corresponding eigenvectors coalesce to one. For \mathcal{PT} -symmetric systems, it turns out that the spontaneous symmetry-breaking points, beyond which the spectrum changes from all real to complex, are just those values at which an EP of the system appears.

The situation is richer when a non-Hermitian system is periodically driven. As discussed above, for the $\omega = 0.5$ resonance, the parameter point $\lambda = 1$ corresponds to the symmetry-breaking point and, consequently, to the EP. Our further numerical investigation shows that for general $\omega = 0.5l$ with integer l , the parameter point $\lambda = 1$ (the real and imaginary parts of the potential depth are equal) is very unique, where the current and the Floquet spectrum behave unexpectedly, regardless of whether $\lambda = 1$ is the symmetry-breaking point. If l is odd, $\lambda = 1$ represents the spontaneous \mathcal{PT} -symmetry-breaking point. However, if l is even, $\lambda = 1$ is below the phase transition point, but it is an EP where the quasienergies and the Floquet states coincide simultaneously. As shown in Fig. 6, for $K = 0.1$ and $\omega = 1$, $\lambda = 1$ (as pointed out in Fig. 1, it is not a symmetry-breaking point) indeed represents an EP, where we observe the two pairs of coincident (identical) Floquet states, corresponding to the degenerate quasienergy -0.498 (upper panels) and the degenerate quasienergy 0.007 (lower panels), respectively. Under such a circumstance, there appears a persistent current with an asymptotically constant value and a power-law increase of the norm $N(t) \propto t^2$ (see Fig. 7), even though $\lambda = 1$ is not the symmetry-breaking point and is deeply rooted in the unbroken- \mathcal{PT} -symmetry regime.

We analytically investigate the current and population behaviors at the exceptional point using a specific driving frequency $\omega = 0.5$. The Schrödinger equation (1) in the momentum representation can be written as

$$i \frac{\partial}{\partial t} c_n = \frac{n^2}{2} c_n + \frac{iK \sin(\omega t)}{2} (\lambda_+ c_{n+1} + \lambda_- c_{n-1}), \quad (15)$$

where c_n denotes the population amplitude on the momentum mode $|n\rangle$ and the coupling coefficients are given by $\lambda_+ = -2i\langle n|f(x)|n+1\rangle$ and $\lambda_- = -2i\langle n|f(x)|n-1\rangle$, with $f(x) = \sin x + i\lambda \cos(x + \phi)$. Since the coupling strength in the hopping direction to the negative momentum state is greater than to the positive momentum state, a negative average current is generally expected. Despite the presence of nonreciprocal hopping in Eq. (15), there is no non-Hermitian skin effect in

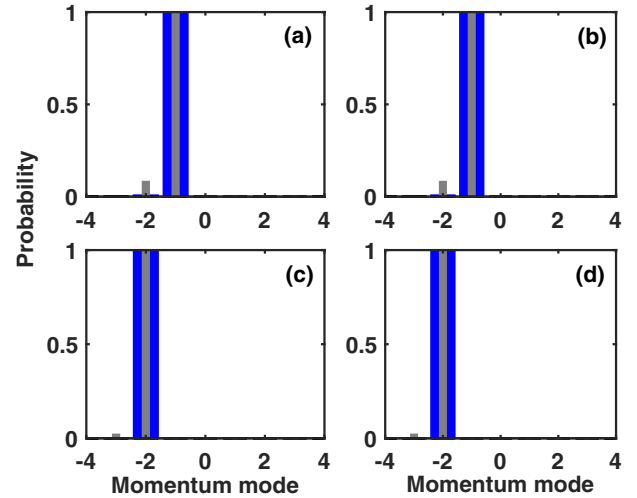


FIG. 6. Probabilities (blue thick bar) and real parts of the probability amplitudes (gray thin bar) in different momentum modes for two pairs of coincident Floquet states, corresponding to quasienergy -0.498 [upper panels (a) and (b)] and 0.007 [lower panels (c) and (d)]. We see that the two quasienergies are identical, and the two Floquet eigenvectors are also completely identical, which is indeed the characteristic of exceptional point (EP) behavior. The parameters are $K = 0.1$, $\omega = 1$, $\lambda = 1$.

the momentum space as in Ref. [75] (where bulk states are localized at the edges in the real space) because the periodicity and the periodic boundary condition in the momentum space are not present due to an extra onsite potential $n^2/2$. However, the nonreciprocal hopping can be used to steer the direction of

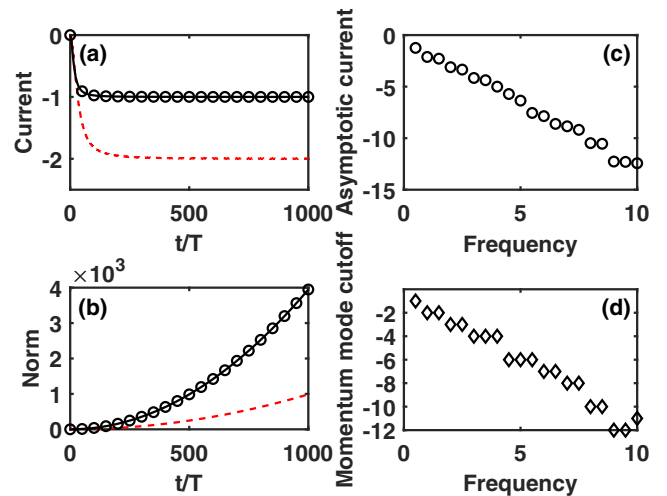


FIG. 7. (a) Time dependence of current $I(t)$ with different parameters $K = 0.01$, $\omega = 0.5$ (solid line) and $K = 0.1$, $\omega = 1$ (dashed line) at EPs. (b) Power-law growth of the norm at EPs, for $K = 0.01$, $\omega = 0.5$ (solid line), and $K = 0.1$, $\omega = 1$ (dashed line). The analytical results (circles) for the norm, predicted by Eq. (19), and for the current, predicted by Eq. (20), agree well with the numerical results. (c) Asymptotic current versus frequency ω at EPs. (d) The momentum mode cutoff (i.e., the maximum attainable negative momentum mode) versus the driving frequency ω at EPs. Here, the EPs correspond to the parameter point $\lambda = 1$ and $\omega = 0.5l$ with integer l .

the ratchet currents. At the exceptional point $\lambda = 1$, Eq. (15) is reduced to

$$i\frac{\partial}{\partial t}c_n = \frac{n^2}{2}c_n + \frac{iK \sin(\omega t)}{2}(\lambda_+c_{n+1}). \quad (16)$$

To be specific, we consider the weakly driven system with the resonance frequency $\omega = 0.5$, starting from the initial state $c_n(0) = \delta_{n,0}$, then the dynamics is limited in the subspace spanned by the basis $|n\rangle = |-1\rangle, |0\rangle, |1\rangle$, and Eq. (16) is truncated to

$$i\frac{\partial}{\partial t} \begin{bmatrix} c_{-1}(t) \\ c_0(t) \\ c_1(t) \end{bmatrix} = \begin{bmatrix} \frac{1}{2} & iK \sin(\omega t) & 0 \\ 0 & 0 & iK \sin(\omega t) \\ 0 & 0 & \frac{1}{2} \end{bmatrix} \begin{bmatrix} c_{-1}(t) \\ c_0(t) \\ c_1(t) \end{bmatrix}. \quad (17)$$

The solution of Eq. (17) can be obtained exactly as follows:

$$\begin{cases} c_{-1}(t) = \frac{iK}{2}te^{-\frac{it}{2}} - iK \sin(\omega t), \\ c_0(t) = 1, \\ c_1(t) = 0, \end{cases} \quad (18)$$

which gives the power-law increase of the norm

$$N(t) \simeq 1 + K^2t^2/4. \quad (19)$$

As time tends to infinity, the asymptotic current reads as

$$I(t \rightarrow \infty) = \lim_{t \rightarrow \infty} \frac{-1}{1 + \frac{4}{K^2t^2}} = -1. \quad (20)$$

Our theoretical prediction is verified by numerical results, as shown in Fig. 7 [see the analytical results (circles) and the numerical results (black solid lines) in Figs. 7(a) and 7(b)]. We also numerically investigate the behavior of the current and the norm for $\omega = 1$, as shown in Figs. 7(a) and 7(b) (see the red dashed lines), where we observe that the magnitude of the asymptotic current is larger than its counterpart for $\omega = 0.5$. This is evident from the fact that for $\omega = 1$, the system can be excited to a higher momentum state $|-2\rangle$. The dependence of the asymptotic current on the resonant frequency ω is also investigated numerically, and it is found in Fig. 7(c) that the asymptotic current increases as the resonant frequency ω increases. Such a dependence stems from the fact that the momentum mode cutoff (i.e., the maximum attainable negative momentum mode) increases with the resonant frequency [see Fig. 7(d)]. In our work, our focus is only on the case of $\phi = 0$. If we set the initial phase $\phi = \pi$, the coupling coefficients are reversed, i.e., $\lambda_+ = 2i\langle n+1|f(x)|n\rangle$ and $\lambda_- = 2i\langle n-1|f(x)|n\rangle$, leading to a positive mean current, which opens an avenue to steer the direction of the directed currents. Such a way of controlling the direction of the ratchet current is essentially based on swapping the nonreciprocal hopping terms in Eq. (15).

To sum up this section, through numerical and analytical investigations, an asymptotic current dependent on a series of discrete frequencies at EPs is revealed, which provides a different type of driving-frequency-dependent current at EPs and broadens the understanding of directed transport at EPs. It should be noted that this type of driving-frequency-dependent asymptotic steady current at EPs depends on the choice of the driving protocol, which is completely different from the

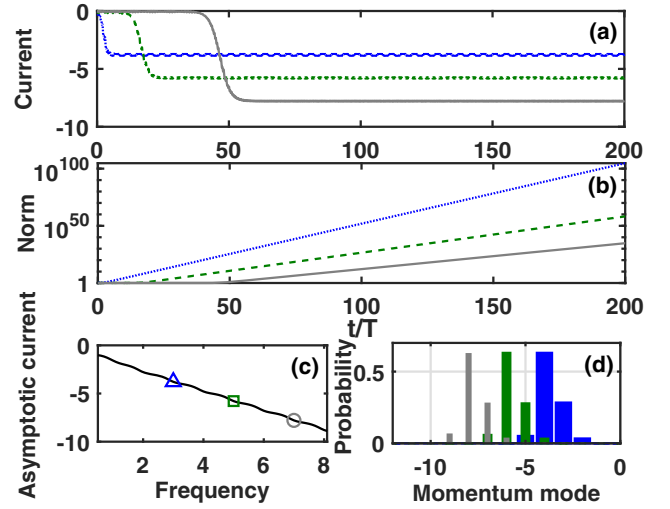


FIG. 8. (a) Time evolution of the current in the broken- \mathcal{PT} -symmetry regime at different driving frequencies, $\omega = 3$ (blue dotted line), $\omega = 5$ (green dashed line), and $\omega = 7$ (gray solid line). (b) Time evolution of the corresponding norms. (c) Asymptotic current versus driving frequency ω . The blue triangle, green square, and gray circle represent the corresponding asymptotic currents [the saturation levels of $I(t)$ with the corresponding colors] in (a). (d) The Floquet eigenstates in the momentum space with the largest imaginary quasienergy for $\omega = 3$ (blue thick bar), $\omega = 5$ (green medium bar), and $\omega = 7$ (gray thin bar), which give rise to the three different asymptotic currents in (c) marked by triangle, square, and circle, respectively. In all plots the parameters are $K = 1$, $\lambda = 1.5$.

staircase growth of the momentum current in the vicinity of EPs previously discovered in the non-Hermitian kicked rotor model [70].

V. \mathcal{PT} -SYMMETRY-BREAKING-INDUCED RATCHET CURRENTS

In this section, we turn our attention to the current dynamics of the broken- \mathcal{PT} -symmetry regime, in which the norm starts to grow exponentially. Figure 8(a) shows the numerical results for the time evolution of the current in the broken- \mathcal{PT} -symmetry regime at different driving frequencies. As we can see, the current evolves to a nonzero asymptotic value for all driving frequencies and the asymptotic current grows as the driving frequency increases, which bears a close resemblance to the current behavior at EPs as shown in Fig. 7(a). The main difference is that for a fixed non-Hermitian parameter, the asymptotic current in the broken- \mathcal{PT} -symmetry regime can be generated for all continuously varying driving frequencies, whereas the asymptotic current at EPs can only be generated for certain discrete driving frequencies. The time evolution of the corresponding norms is illustrated in Fig. 8(b), where we observe that the norm grows exponentially and accelerates as the driving frequency increases. The enhancement of the asymptotic current by increasing the driving frequency is more clearly demonstrated in Fig. 8(c). In Fig. 8(c), we see that the value of asymptotic current increases almost linearly with the driving frequency.

The mechanism of the generation of the asymptotic current in the broken- \mathcal{PT} -symmetry regime can be understood as

follows. At the initial time, an arbitrary state can be expanded on the basis of the Floquet eigenstates, namely,

$$|\psi(0)\rangle = \sum_{\alpha} C_{\alpha} |\phi_{\alpha}(0)\rangle, \quad (21)$$

where C_{α} are the amplitudes for the Floquet eigenstates $|\phi_{\alpha}(0)\rangle$. With the time evolution, the quantum state takes the form of $|\psi(t)\rangle = \sum_{\alpha} C_{\alpha} e^{-i\varepsilon_{\alpha}t} |\phi_{\alpha}(t)\rangle$. In the broken- \mathcal{PT} -symmetry regime, the quasienergy is complex, i.e., $\varepsilon_{\alpha} = \varepsilon_{\alpha}^r + i\varepsilon_{\alpha}^i$. Accordingly, we have

$$|\psi(t)\rangle = \sum_{\alpha} C_{\alpha} e^{-i\varepsilon_{\alpha}^r t + \varepsilon_{\alpha}^i t} |\phi_{\alpha}(t)\rangle. \quad (22)$$

As time increases, the component $C_{\alpha} \exp(\varepsilon_{\alpha}^i t)$ with $\varepsilon_{\alpha}^i > 0$ grows exponentially and that with $\varepsilon_{\alpha}^i < 0$ decays, so that the quantum state $|\psi(t)\rangle$ eventually evolves to the Floquet eigenstate with the maximum ε_{α}^i . Thus, the mean momentum $\langle p \rangle$ corresponding to these Floquet eigenstates with maximum ε_{α}^i is the main contributor to the current. To confirm our analysis, in Fig. 8(d) we present numerically the momentum distributions of the Floquet eigenstates with maximum ε_{α}^i for three different driving frequencies (marked by thick, medium, and thin bars with different colors). A detailed inspection shows that the mean momentum $\langle p \rangle$ corresponding to these Floquet eigenstates increases as the driving frequency increases, and shifts to larger negative values, with each mean momentum having a one-to-one correspondence with the asymptotic current as shown in Fig. 8(a).

Same as in the unbroken- \mathcal{PT} -symmetry regime, we find that most of the Floquet eigenstates in the broken- \mathcal{PT} -symmetry regime are degenerate and well localized in the momentum space, which results in that Floquet eigenstates with the largest ε_{α}^i always appear in pairs as shown in Figs. 9(a)–9(c). Interestingly, we find that when the driving frequency is below a certain threshold ω_c , these two Floquet eigenstates occupy the same momentum modes (that is, the population probabilities in the momentum modes are identical) with a nonzero and negative mean momentum. This leads to a stable negative asymptotic current. When the driving frequency is above the threshold, i.e., $\omega > \omega_c$, these two degenerate Floquet eigenstates begin to gradually separate from each other. As ω increases, these two Floquet eigenstates become more and more separated and populate the momentum modes in an almost symmetrical manner: one with a positive mean momentum and the other with a negative mean momentum. Due to the linear superposition of these two different degenerate eigenstates with the largest ε_{α}^i , the initial state evolves into one of the two degenerate eigenstates with unpredictability. This means that the system will randomly settle into one of the two different degenerate eigenstates with the largest ε_{α}^i , leading to an unpredictability of the current direction. Thus, to achieve a stable asymptotic current, we should limit the driving frequency to less than the threshold value, i.e., $\omega < \omega_c$. The phase diagram of the frequency threshold ω_c in the (K, λ) space is plotted in Fig. 9(d). It can be observed that the threshold value increases with both the driving amplitude K and the non-Hermitian parameter λ .

We would like to point out that the finding that the asymptotic current increases with successive increases in the driving frequency in the broken- \mathcal{PT} -symmetry phase is truly unique

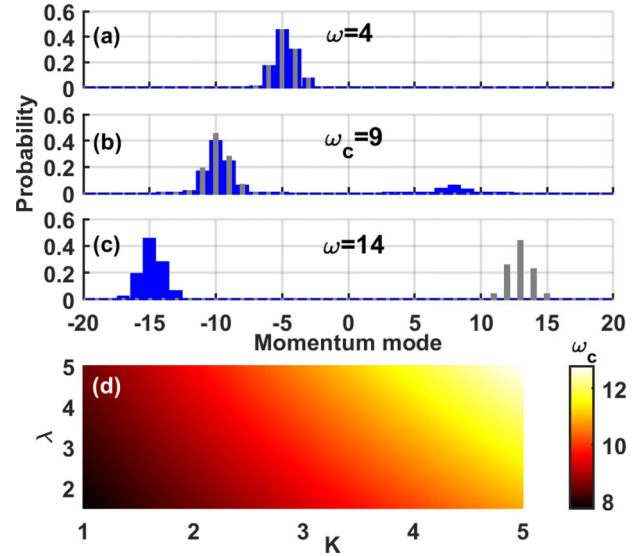


FIG. 9. Momentum distributions of the three pairs of degenerate Floquet states with the largest imaginary value of the quasienergy, for (a) $\omega = 4 < \omega_c$, (b) $\omega_c = 9$, and (c) $\omega = 15 > \omega_c$. Here, a pair of degenerate Floquet states are represented by blue thick and light gray thin bars. The other parameters are $K = \lambda = 2$ which correspond to a broken- \mathcal{PT} -symmetry phase. (d) Threshold frequency ω_c , corresponding to the appearance of the separation of the momentum distribution of the degenerate Floquet eigenstates with the largest imaginary part of the quasienergy, as a function of the driving amplitude K and the non-Hermitian strength λ . The different map colors specify different values of ω_c .

to the time-continuous driving system and is not accessible in the non-Hermitian kicked rotor system with \mathcal{PT} -symmetric driving potential [70].

VI. NONLINEARITY EFFECTS ON THE NON-HERMITIAN CURRENTS

Finally, we address the impact of interatomic interactions on the current behaviors, with particular emphasis on the dynamics at the EPs. As mentioned above, for EPs in the noninteracting case, the current tends asymptotically to a constant value and the norm shows a power-law growth. First of all, we consider the parameters $\lambda = 1$ and $\omega = 1$, corresponding to the EP for the noninteracting case $g = 0$, which is below the symmetry-breaking point and is rooted in the unbroken- \mathcal{PT} -symmetry regime. In this case, the effects of nonlinearity on the directed current can be visualized in Fig. 10. In Fig. 10, the top row shows the time evolution of the populations in momentum space, and the middle and bottom rows show the respective currents and norms. For small $g = 0.01$ [see Figs. 10(a), 10(d), and 10(g)], the current oscillates periodically with time, acting like the resonant current in the unbroken- \mathcal{PT} -symmetry regime as shown in Fig. 3(a). As g increases (from the left column to the right column), we see that the coupling between the initial state $|0\rangle$ and other momentum states is gradually suppressed, so that the oscillatory amplitudes of the currents and norms are progressively reduced, manifesting a self-trapping phenomenon in the

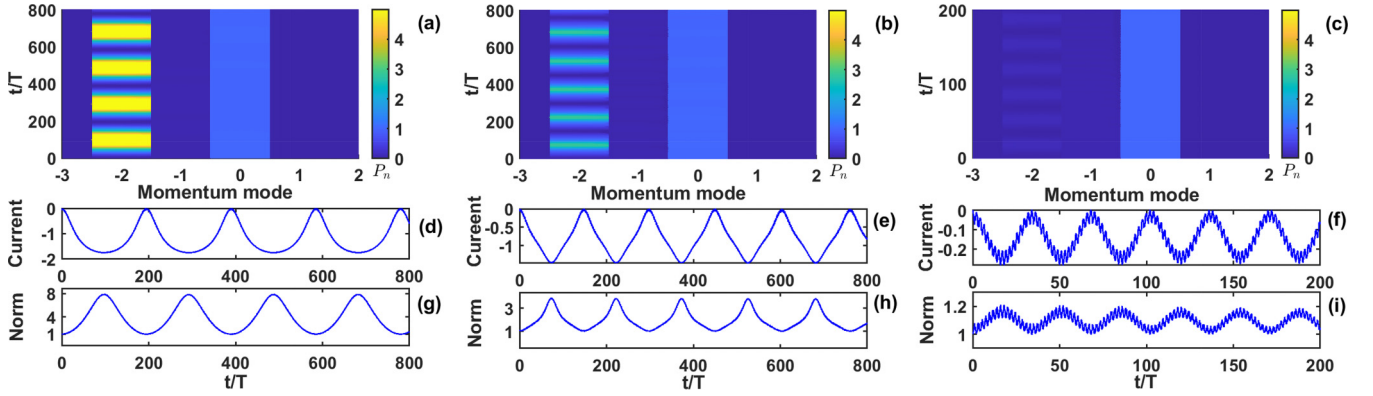


FIG. 10. The nonlinearity effects on the directed currents at EP with $K = 0.1$, $\omega = 1$, $\lambda = 1$, starting from the initial state $|0\rangle$. Top panels: time evolution of the populations in momentum space. Middle panels: time evolution of current $I(t)$. Bottom panels: time evolution of norm $N(t)$. From the left to the right column: $g = 0.01, 0.1, 0.2$. In (a)–(c), the color bar indicates the population P_n in the momentum mode $|n\rangle$.

momentum space due to the presence of nonlinearity. However, the dynamics are quite different for $\lambda = 1$ and $\omega = 0.5$ that correspond to the symmetry-breaking point in the noninteracting case. At $g = 0.01$ [see Figs. 11(a), 11(d), and 11(g)], the quadratic growth of the norm is suppressed to some extent, and the current $I(t)$ oscillates nonperiodically with time. As the nonlinear strength g increases to 0.1 [see Figs. 11(b), 11(e), and 11(h)], the aperiodic oscillation of current and norm becomes more pronounced. Particularly, there also exists an asymptotic current as g continues to increase [see Figs. 11(c), 11(f), and 11(i)]. The appearance of the asymptotic current is caused by the nonlinearity-induced \mathcal{PT} -symmetry breaking, and the population in the momentum mode $|0\rangle$ also grows with time due to the nonlinear cross coupling of the momentum modes. This contrasts sharply with the noninteracting system, where the population of momentum mode $|0\rangle$ remains constant because the coupling $\lambda_- = \langle n|\hat{V}|n-1\rangle$ vanishes at EP with $\lambda = 1$ and the asymptotic current is induced by the EP. In this work, we have only addressed how nonlinearity affects the current behavior of EP in its linear counterpart. When other parameter ranges are taken into account, the corresponding current behavior should be much richer and deserves to be explored in more detail in the future.

VII. CONCLUSION

To conclude, we report on the non-Hermitian ratchet currents in a \mathcal{PT} -symmetric Floquet system with symmetric harmonic driving. The main results of the ratchet current are presented in Table I. In the exact \mathcal{PT} -symmetry phase, for a finite set of resonant frequencies, we show how a long-lasting ratchet current arises from the non-Hermiticity. We show that increasing the non-Hermitian strength can enhance the resonant currents, providing a means of controlling the directed current for smooth continuous driving which has hitherto been studied in the Hermitian system. The resonant currents exist only when the non-Hermitian strength does not vanish, so that they are indeed a signature of non-Hermitian directed transport. The non-Hermitian resonant current reaches the largest negative value when the real and imaginary parts of the potential depth are equal, i.e., $\lambda = 1$, where the stable asymptotic current occurs owing to the exceptional points (EPs) mechanism. When $\lambda = 1$, we find that EPs occur at the driving frequency of integer or half-integer values. More interestingly, the asymptotic current at EPs can occur below the phase transition (symmetry-breaking) threshold because such driving frequencies (e.g., $\omega = 1$) of EPs, corresponding to the second-order resonance, lie in an isolated point

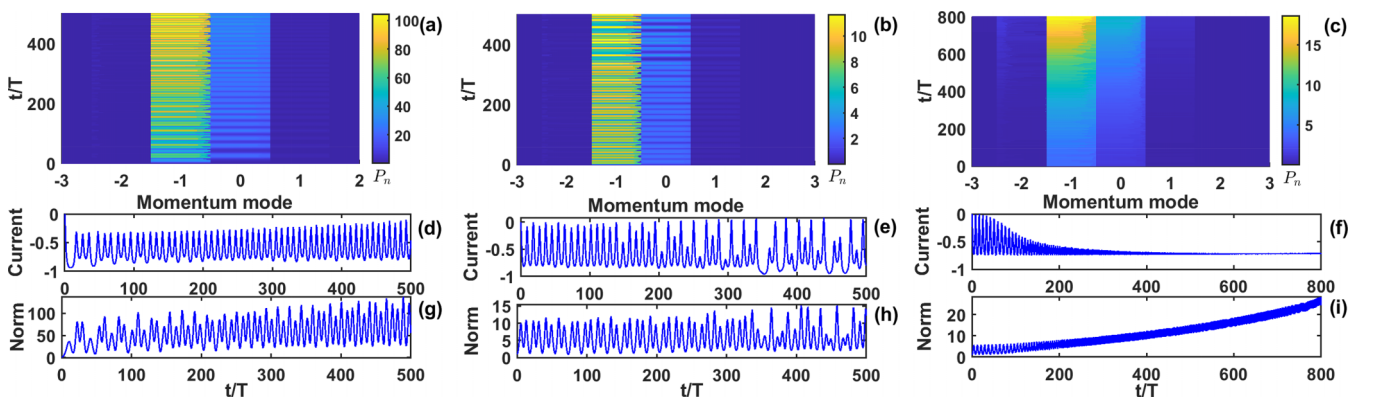


FIG. 11. The nonlinearity effects on the directed currents for the same set of parameters as in Fig. 10, but with $\omega = 0.5$. From the left to the right column, the nonlinearity strengths are $g = 0.01, 0.1, 0.4$. In (a)–(c), the color bar indicates the population P_n in the momentum mode $|n\rangle$.

TABLE I. Summary of main characteristics of currents and their physical mechanisms in different phase domains (invariant \mathcal{PT} symmetry, exceptional point, broken and nonlinear \mathcal{PT} symmetry).

| Phase | Unbroken- \mathcal{PT} -symmetry phase | EPs | Broken- \mathcal{PT} -symmetry phase | Nonlinear |
|--|--|--|--|---|
| Main characteristics of currents | At resonance, the current oscillates with time and the time-averaged current reaches its maximum value | Stable asymptotic currents appear and increase as the resonance frequency is increased | As the driving frequency is successively increased, the asymptotic current increases | Suppression or enhancement of directed currents by nonlinearity |
| Physical origins of current generation | Coupling of the initial state to the resonant current-carrying states | The singularity of Hamiltonian in momentum space | The dominance of the Floquet state with the maximum imaginary value of the quasienergy over the dynamics | Self-trapping effect in the momentum space and nonlinearity-induced \mathcal{PT} -symmetry breaking |

in the unbroken- \mathcal{PT} -symmetry regime. For weak driving, an effectively non-Hermitian three-level model is developed, which shows excellent agreement with the direct numerical results, even in the broken- \mathcal{PT} -symmetry regime for the first-order resonance. Moreover, there also exist asymptotic currents in the broken- \mathcal{PT} -symmetry phase, which have a different physical mechanism from the ones at the EPs. The directed currents resulting from the \mathcal{PT} -symmetry breaking are the consequence of the predominance of the Floquet state with the maximum imaginary value of the quasienergy over the dynamics of the non-Hermitian system. Interestingly, the momentum mode cutoff (the maximum attainable negative momentum eigenstate) of the Floquet states with the largest imaginary value of the quasienergy increases as the frequency is continuously increased, leading to an increase in the asymptotic current with the driving frequency. Finally, we consider the effect of the nonlinear interaction on the currents in the parameter configurations where the corresponding linear system lies at the EPs. It is shown that the nonlinearity can either destroy the ratchet effect due to the self-trapping in the momentum space, or induce a stable asymptotic current due to the nonlinearly induced \mathcal{PT} -symmetry breaking. Since the non-Hermitian Hamiltonian can be used to describe nonequilibrium relaxation problems, optical wave transport in dissipative media, exciton-polariton condensate systems, etc., our results may open new perspectives and applications of ratchet effects in a variety of non-Hermitian systems.

In the Hermitian system, in order to generate the ratchet current, one must choose a sawtoothlike asymmetric temporal driving (e.g., two-frequency driving) to break both the time-reversal and the space-inversion symmetries. However, our study shows that even a single-frequency temporal driving can produce a ratchet current in the non-Hermitian system. The unique feature of using non-Hermitian driving to generate ratchet currents is that no sawtoothlike asymmetric temporal driving is required. Instead, a simple harmonic driving field is sufficient. As was done in Ref. [76], a model that links the Gross-Pitaevskii mean-field equation with an additional imaginary potential to the Lindblad master equation was established theoretically and justified experimentally, thus providing a basis for the study of the ratchet current in the open system. At present, there is still a lack of complete

knowledge about the ratchet currents in more realistic open systems, and this deserves to be further investigated from the perspective of the Lindblad master equation.

ACKNOWLEDGMENTS

The work was supported by the National Natural Science Foundation of China (Grants No. 12375022 and No. 11975110), the Natural Science Foundation of Zhejiang Province (Grant No. LY21A050002), and Zhejiang Sci-Tech University Scientific Research Start-up Fund (Grant No. 20062318-Y).

APPENDIX

In this Appendix, we give a detailed derivation of the effective three-level model (10) in the main text for the weakly driven system under resonance. For a time-periodic Hamiltonian, there exists a complete set of solutions of the form $|\phi_\alpha(t)\rangle = e^{-i\varepsilon_\alpha t}|u_\alpha(t)\rangle$, where the Floquet states inherit the period of the driving, satisfying $|u_\alpha(t)\rangle = |u_\alpha(t+T)\rangle$, which can be obtained by solving the eigenvalue equation $[\hat{H}(t) - i\frac{\partial}{\partial t}]|u_\alpha(t)\rangle = \varepsilon_\alpha|u_\alpha(t)\rangle$. Note that the quasienergies and the Floquet states in the solution $|\phi_\alpha(t)\rangle$ are not uniquely defined. If $|u_\alpha(t)\rangle$ are the eigenstates of the eigenvalue equation with eigenvalue ε_α , then the replacement

$$\varepsilon_{\alpha m} = \varepsilon_\alpha - m\omega, \quad |u_{\alpha m}(t)\rangle = |u_\alpha(t)\rangle e^{-im\omega t} \quad (\text{A1})$$

yields a new set of quasienergies and Floquet states corresponding to the same solution $|\phi_\alpha(t)\rangle = |u_\alpha(t)\rangle e^{-i\varepsilon_\alpha t} = |u_{\alpha m}(t)\rangle e^{-i\varepsilon_{\alpha m} t}$, satisfying

$$\left[\hat{H}(t) - i\frac{\partial}{\partial t} \right] |u_{\alpha m}(t)\rangle = \varepsilon_{\alpha m} |u_{\alpha m}(t)\rangle. \quad (\text{A2})$$

For unperturbed system in the extended Hilbert space, Eq. (A2) reads as

$$\left(\frac{\hat{p}^2}{2} - i\frac{\partial}{\partial t} \right) u_{nm}^0(x, t) = \varepsilon_{nm}^0 u_{nm}^0(x, t), \quad (\text{A3})$$

where unperturbed Floquet states read as

$$u_{nm}^0(x, t) = \langle x, t | n, m \rangle = \frac{1}{\sqrt{2\pi T}} \exp(inx - im\omega t), \quad (\text{A4})$$

with the zeroth-order quasienergy

$$\varepsilon_{nm}^0 = \frac{n^2}{2} - m\omega. \quad (\text{A5})$$

In the following, we will concentrate on the resonance condition, defined as

$$\frac{n^2}{2} = m\omega, \quad (\text{A6})$$

where the unperturbed Floquet states $|n, m\rangle$ are degenerate with $\varepsilon_{nm}^0 = 0$ and we expect the largest value of the ratchet current to appear.

These degenerate resonant states are connected by the driving. The periodic driving can be expanded as Fourier components

$$\hat{V}(x, t) = \frac{K}{4}(\lambda_- e^{ix} + \lambda_+ e^{-ix})(e^{i\omega t} - e^{-i\omega t}). \quad (\text{A7})$$

We can rewrite (A7) in the extended Hilbert space using the unperturbed Floquet basis $|n, m\rangle$,

$$\begin{aligned} \hat{V} = \frac{K}{4} \sum_{n,m=-\infty}^{\infty} [& (\lambda_- (|n+1, m+1\rangle\langle n, m| \\ & - |n+1, m\rangle\langle n, m+1|) + \lambda_+ (|n, m+1\rangle\langle n+1, m| \\ & - |n, m\rangle\langle n+1, m+1|)]. \end{aligned} \quad (\text{A8})$$

According to the perturbative method, the effective dynamics up to the second order can be described by an effective T matrix with the matrix elements

$$\begin{aligned} \langle n, m | \hat{T} | n', m' \rangle \\ \simeq \langle n, m | \hat{V} | n', m' \rangle + \sum_{n'', m''} \frac{\langle n, m | \hat{V} | n'', m'' \rangle \langle n'', m'' | \hat{V} | n', m' \rangle}{-\varepsilon_{n'', m''}^0}. \end{aligned} \quad (\text{A9})$$

Let us first focus on the case $\omega = 1$, which specifies the resonance condition $\frac{n^2}{2} = m\omega$ with $m = 2$ and $n = \pm 2$, and

take it as an example to illustrate this perturbative analysis method. The resonant states $\{|2, 2\rangle, |0, 0\rangle, |\bar{2}, 2\rangle\}$ are “degenerate” with quasienergy $\varepsilon = 0$ and are connected under the effect of driving. The T -matrix elements for the second-order dynamics, spanning the space $(\{|2, 2\rangle, |0, 0\rangle, |\bar{2}, 2\rangle\})$, can be calculated as follows. There is no direct coupling between the initial state $|0, 0\rangle$ and $|2, 2\rangle, |\bar{2}, 2\rangle$, i.e., $\langle 0, 0 | \hat{V} | 2, 2 \rangle = \langle 0, 0 | \hat{V} | \bar{2}, 2 \rangle = 0$. The second-order mixing between $|0, 0\rangle$ and $|2, 2\rangle, |\bar{2}, 2\rangle$ is generated by virtual intermediate states $|1, 1\rangle$ and $|\bar{1}, 1\rangle$. Thus, all matrix elements $\langle n, m | \hat{T} | n', m' \rangle$ can be calculated as

$$\langle 2, 2 | \hat{T} | 0, 0 \rangle = \frac{\langle 2, 2 | \hat{V} | 1, 1 \rangle \langle 1, 1 | \hat{V} | 0, 0 \rangle}{-\varepsilon_{11}^0} = \frac{K^2 \lambda_-}{8}, \quad (\text{A10})$$

$$\langle 0, 0 | \hat{T} | 2, 2 \rangle = \frac{\langle 0, 0 | \hat{V} | 1, 1 \rangle \langle 1, 1 | \hat{V} | 2, 2 \rangle}{-\varepsilon_{11}^0} = \frac{K^2 \lambda_+}{8}, \quad (\text{A11})$$

$$\langle 0, 0 | \hat{T} | \bar{2}, 2 \rangle = \langle 2, 2 | \hat{T} | 0, 0 \rangle = \frac{K^2 \lambda_-}{8}, \quad (\text{A12})$$

$$\langle \bar{2}, 2 | \hat{T} | 0, 0 \rangle = \langle 0, 0 | \hat{T} | 2, 2 \rangle = \frac{K^2 \lambda_+}{8}, \quad (\text{A13})$$

with the remaining matrix elements being all zero. Restricted to these second-order matrix elements, in the space spanned only by the Floquet states $\{|2, 2\rangle, |0, 0\rangle, |\bar{2}, 2\rangle\}$ (using this ordering), the effective three-level model is given by the matrix

$$T \simeq \begin{bmatrix} 0 & \frac{K^2 \lambda_-}{8} & 0 \\ \frac{K^2 \lambda_+}{8} & 0 & \frac{K^2 \lambda_-}{8} \\ 0 & \frac{K^2 \lambda_+}{8} & 0 \end{bmatrix}, \quad (\text{A.14})$$

which corresponds to Eq. (10) in the main text.

Following the same procedure as above, under the resonance condition $\frac{n^2}{2} = m\omega$, we can construct the effective three-level model for the $\omega = 0.5$ resonance, with the matrix defined by Eq. (13) in the main text, which only involves the first-order transition between the resonant Floquet states $\{|1, 1\rangle, |0, 0\rangle, |\bar{1}, 1\rangle\}$.

-
- [1] J. Gong and P. Brumer, *Phys. Rev. E* **70**, 016202 (2004); *Phys. Rev. Lett.* **97**, 240602 (2006).
- [2] S. Denisov, L. Morales-Molina, S. Flach, and P. Hänggi, *Phys. Rev. A* **75**, 063424 (2007).
- [3] S. Denisov, L. Morales-Molina, and S. Flach, *Europhys. Lett.* **79**, 10007 (2007).
- [4] S. Denisov, S. Flach, and P. Hänggi, *Phys. Rep.* **538**, 77 (2014).
- [5] T. Salger, S. Kling, T. Hecking, C. Geckeler, L. Morales-Molina, and M. Weitz, *Science* **326**, 1241 (2009).
- [6] Y. V. Gulyaev, A. S. Bugaev, V. M. Rozenbaum, and L. I. Trakhtenberg, *Phys. Usp.* **63**, 311 (2020).
- [7] A. Hashemi, M. Tahernia, T. C. Hui, W. D. Ristenpart, and G. H. Miller, *Phys. Rev. E* **105**, 065001 (2022).
- [8] R. W. Simmonds, A. Marchenkov, E. Hoskinson, J. C. Davis, and R. E. Packard, *Nature (London)* **412**, 55 (2001).
- [9] Y.-J. Wang, D. Z. Anderson, V. M. Bright, E. A. Cornell, Q. Diot, T. Kishimoto, M. Prentiss, R. A. Saravanan, S. R. Segal, and S. Wu, *Phys. Rev. Lett.* **94**, 090405 (2005).
- [10] B. T. Seaman, M. Kramer, D. Z. Anderson, and M. J. Holland, *Phys. Rev. A* **75**, 023615 (2007).
- [11] S. Flach, O. Yevtushenko, and Y. Zolotaryuk, *Phys. Rev. Lett.* **84**, 2358 (2000).
- [12] P. Reimann, *Phys. Rev. Lett.* **86**, 4992 (2001).
- [13] P. Hänggi and F. Marchesoni, *Rev. Mod. Phys.* **81**, 387 (2009).
- [14] E. Lundh and M. Wallin, *Phys. Rev. Lett.* **94**, 110603 (2005).
- [15] M. Sadgrove, M. Horikoshi, T. Sekimura, and K. Nakagawa, *Phys. Rev. Lett.* **99**, 043002 (2007).
- [16] A. Kenfack, J. Gong, and A. K. Pattanayak, *Phys. Rev. Lett.* **100**, 044104 (2008).
- [17] D. H. White, S. K. Ruddell, and M. D. Hoogerland, *Phys. Rev. A* **88**, 063603 (2013).
- [18] J. Ni, W. K. Lam, S. Dadrás, M. F. Borunda, S. Wimberger, and G. S. Summy, *Phys. Rev. A* **94**, 043620 (2016).
- [19] C. Hainaut, A. Rancon, J.-F. Clément, J. C. Garreau, P. Szriftgiser, R. Chicireanu, and D. Delande, *Phys. Rev. A* **97**, 061601(R) (2018).
- [20] F. L. Moore, J. C. Robinson, C. Bharucha, P. E. Williams, and M. G. Raizen, *Phys. Rev. Lett.* **73**, 2974 (1994).
- [21] M. Heimsoth, C. E. Creffield, and F. Sols, *Phys. Rev. A* **82**, 023607 (2010).

- [22] D. Poletti, G. Benenti, G. Casati, P. Hänggi, and B. Li, *Phys. Rev. Lett.* **102**, 130604 (2009).
- [23] C. E. Creffield and F. Sols, *Phys. Rev. Lett.* **103**, 200601 (2009).
- [24] D. Poletti, G. Benenti, G. Casati, and B. Li, *Phys. Rev. A* **76**, 023421 (2007).
- [25] W. L. Zhao, L. B. Fu, and J. Liu, *Phys. Rev. E* **90**, 022907 (2014).
- [26] T. S. Monteiro, A. Rancon, and J. Ruostekoski, *Phys. Rev. Lett.* **102**, 014102 (2009).
- [27] L. Morales-Molina and S. Flach, *New J. Phys.* **10**, 013008 (2008).
- [28] C. M. Bender and S. Boettcher, *Phys. Rev. Lett.* **80**, 5243 (1998).
- [29] I. Rotter, *J. Phys. A: Math. Theor.* **42**, 153001 (2009).
- [30] C. M. Bender, D. C. Brody, and H. F. Jones, *Phys. Rev. Lett.* **89**, 270401 (2002).
- [31] C. M. Bender, D. C. Brody, and H. F. Jones, *Am. J. Phys.* **71**, 1095 (2003).
- [32] S. Weigert, *Phys. Rev. A* **68**, 062111 (2003).
- [33] K. G. Makris, R. El-Ganainy, D. N. Christodoulides, and Z. H. Musslimani, *Phys. Rev. A* **81**, 063807 (2010).
- [34] A. A. Zyablovsky, A. P. Vinogradov, A. A. Pukhov, A. V. Dorofeenko, and A. A. Lisyansky, *Phys. Usp.* **57**, 1063 (2014).
- [35] J. Doppler, A. A. Mailybaev, J. Böhm, U. Kuhl, A. Girschik, F. Libisch, T. J. Milburn, P. Rabl, N. Moiseyev, and S. Rotter, *Nature (London)* **537**, 76 (2016).
- [36] Q. Xie, S. Rong, and X. Liu, *Phys. Rev. A* **98**, 052122 (2018).
- [37] D. Halpern, H. Li, and T. Kottos, *Phys. Rev. A* **97**, 042119 (2018).
- [38] M. Parto, Y. G. N. Liu, B. Bahari, M. Khajavikhan, and D. N. Christodoulides, *Nanophotonics* **10**, 403 (2020).
- [39] M.-A. Miri and A. Alú, *Science* **363**, eaar7709 (2019).
- [40] H. Hodaie, A. U. Hassan, S. Wittek, H. Garcia-Gracia, R. El-Ganainy, D. N. Christodoulides, and M. Khajavikhan, *Nature (London)* **548**, 187 (2017).
- [41] C. Chen, L. Jin, and R.-B. Liu, *New J. Phys.* **21**, 083002 (2019).
- [42] B. Zhen, C. W. Hsu, Y. Igarashi, L. Lu, I. Kaminer, A. Pick, S.-L. Chua, J. D. Joannopoulos, and M. Soljačić, *Nature (London)* **525**, 354 (2015).
- [43] Z. Lin, H. Ramezani, T. Eichelkraut, T. Kottos, H. Cao, and D. N. Christodoulides, *Phys. Rev. Lett.* **106**, 213901 (2011).
- [44] L. Feng, Y.-L. Xu, W. S. Fegadolli, M.-H. Lu, J. E. B. Oliveira, V. R. Almeida, Y.-F. Chen, and A. Scherer, *Nat. Mater.* **12**, 108 (2013).
- [45] W. D. Heiss, *J. Phys. A: Math. Theor.* **45**, 444016 (2012).
- [46] C. T. West, T. Kottos, and T. Prosen, *Phys. Rev. Lett.* **104**, 054102 (2010).
- [47] N. Moiseyev, *Phys. Rev. A* **83**, 052125 (2011).
- [48] X. Luo, J. Huang, H. Zhong, X. Qin, Q. Xie, Y. S. Kivshar, and C. Lee, *Phys. Rev. Lett.* **110**, 243902 (2013).
- [49] Y. N. Joglekar, R. Marathe, P. Durganandini, and R. K. Pathak, *Phys. Rev. A* **90**, 040101(R) (2014).
- [50] J. Gong and Q.-h. Wang, *Phys. Rev. A* **91**, 042135 (2015).
- [51] S. Longhi, *J. Phys. A: Math. Theor.* **50**, 505201 (2017).
- [52] Y. Wu, B. Zhu, S.-F. Hu, Z. Zhou, and H.-H. Zhong, *Front. Phys.* **12**, 121102 (2017).
- [53] X. B. Luo, B. Y. Yang, X. F. Zhang, L. Li, and X. G. Yu, *Phys. Rev. A* **95**, 052128 (2017).
- [54] M. Chitsazi, H. Li, F. M. Ellis, and T. Kottos, *Phys. Rev. Lett.* **119**, 093901 (2017).
- [55] N. Wang, Z.-Q. Zhang, and C. T. Chan, *Phys. Rev. B* **98**, 085142 (2018).
- [56] L. Zhou and J. Gong, *Phys. Rev. B* **98**, 205417 (2018).
- [57] Z. Turker, S. Tombuloglu, and C. Yuce, *Phys. Lett. A* **382**, 2013 (2018).
- [58] L. Zhou and J. Pan, *Phys. Rev. A* **100**, 053608 (2019).
- [59] D.-J. Zhang, Q.-h. Wang, and J. Gong, *Phys. Rev. A* **100**, 062121 (2019).
- [60] J. Li, A. K. Harter, J. Liu, L. de Melo, Y. N. Joglekar, and L. Luo, *Nat. Commun.* **10**, 855 (2019).
- [61] L. Zhou, *Phys. Rev. B* **100**, 184314 (2019).
- [62] S. Mudute-Ndumbe and E.-M. Graefe, *New J. Phys.* **22**, 103011 (2020).
- [63] H. Wu and J.-H. An, *Phys. Rev. B* **102**, 041119(R) (2020).
- [64] B. Zhu, H. Zhong, J. Jia, F. Ye, and L. Fu, *Phys. Rev. A* **102**, 053510 (2020).
- [65] L. Ding, K. Shi, Q. Zhang, D. Shen, X. Zhang, and W. Zhang, *Phys. Rev. Lett.* **126**, 083604 (2021).
- [66] L. Zhou and W. Han, *Phys. Rev. B* **106**, 054307 (2022).
- [67] W.-L. Zhao, *Phys. Rev. Res.* **4**, 023004 (2022).
- [68] L. Zhou and D.-J. Zhang, *Entropy* **25**, 1401 (2023).
- [69] S. Longhi, *Phys. Rev. A* **95**, 012125 (2017).
- [70] W. L. Zhao, J. Wang, X. Wang, and P. Tong, *Phys. Rev. E* **99**, 042201 (2019).
- [71] J.-Z. Li, W.-L. Zhao, and J. Liu, *Phys. Rev. A* **107**, 032208 (2023).
- [72] G. Lyu and G. Watanabe, *Phys. Rev. A* **105**, 023328 (2022).
- [73] J. H. Noble, M. Lubasch, and U. D. Jentschura, *Eur. Phys. J. Plus* **128**, 93 (2013).
- [74] J. H. Noble, M. Lubasch, J. Stevens, and U. D. Jentschura, *Comput. Phys. Commun.* **221**, 304 (2017).
- [75] S. Yao and Z. Wang, *Phys. Rev. Lett.* **121**, 086803 (2018).
- [76] G. Barontini, R. Labouvie, F. Stubenrauch, A. Vogler, V. Guarrera, and H. Ott, *Phys. Rev. Lett.* **110**, 035302 (2013).